Available online at www.sciencedirect.com
SCIENCE DIRECT®
Catalysis Today 93–95 (2004) 493–503
CATALYSIS TODAY
www.elsevier.com/locate/cattod

Comparative studies on catalytic behaviors of various Co- and Ni-based catalysts during liquid phase acetonitrile hydrogenation

Hexing Li [a,*], Yuedong Wu [a], Ying Wan [a], Jing Zhang [a], Weilin Dai [b], Minghua Qiao [b]

[a] *Department of Chemistry, Shanghai Normal University, Shanghai 200234, PR China*
[b] *Department of Chemistry, Fudan University, Shanghai 200433, PR China*

Available online 28 July 2004

Abstract

The Ni-B and Co-B amorphous alloys exhibited much higher activity and selectivity to ethylamine ($C_2H_5NH_2$) than their corresponding crystallized counterparts and Raney Ni during liquid phase hydrogenation of acetonitrile (CH_3CN). In comparison with the Ni-B amorphous alloy, the Co-B amorphous alloy exhibited longer lifetime and better selectivity, though its activity was slightly lower. The maximum yield of $C_2H_5NH_2$ could reach 93.5%, showing a good potential in industrial application. The higher activity of the amorphous alloys could be attributed to the large active surface area, the unique amorphous structure together with the suitable structural parameters, and the electron donation of the alloying B to the metallic Ni or Co. The resulted electron-enriched metallic active sites may also account for the better selectivity to $C_2H_5NH_2$ of the amorphous alloys since, on one hand, it could promote the hydrogenation of $CH_3CH{=}NH$ toward $C_2H_5NH_2$ by activating the C=N bond; and on the other hand, it may retard the condensation between $CH_3CH{=}NH$ and $C_2H_5NH_2$ leading to $(C_2H_5)_2NH$ by inhibiting the adsorption of $C_2H_5NH_2$ which was essential for the condensation. The Co-B amorphous alloy was more selective than the Ni-B owing to its stronger adsorption for CH_3CN and the higher electron density on the Co active sites, both of them could inhibit the adsorption for $C_2H_5NH_2$ and in turn, retard the condensation. This could also account for its longer lifetime. However, such stronger adsorption for CH_3CN was harmful for the competitive adsorption for hydrogen and in turn resulted in a slightly lower hydrogenation activity than the Ni-B since the CH_3CN hydrogenation was first-order with respect to hydrogen while zero-order to CH_3CN.
© 2004 Elsevier B.V. All rights reserved.

Keywords: Co-B and Ni-B amorphous alloys; Raney Ni; Acetonitrile (CH_3CN); Selective hydrogenation; Ethylamine ($C_2H_5NH_2$)

1. Introduction

Ethylamine ($C_2H_5NH_2$) is an important starting material or intermediate for the production of diverse pesticides, rubber promoters, ion-exchanging resins, anti-oxidation agents, and surfactants, etc. Although most amines are industrially produced via selective hydrogenation of the corresponding nitriles [1], traditionally, large volume of $C_2H_5NH_2$ is always produced through the reaction between ethanol and liquid ammonia, possibly due to the high cost and non-availability of CH_3CN at early times. Recently, with the rapid development of the acrylonitrile industry, a large quantity of CH_3CN was accumulated since it is a main byproduct during the acrylonitrile production (10% (w/w)). As CH_3CN is only seldom used as an organic solvent, there is a strong driving force to develop its new application area. One promising way is the hydrogenation of CH_3CN to produce more useful $C_2H_5NH_2$. In comparison with the traditional method, the production of $C_2H_5NH_2$ via CH_3CN hydrogenation possesses the superiority in saving resources, reducing waste disposal and protecting the environment. However, the hydrogenation of nitriles is relatively complex since primary amine, secondary amine, tertiary amine and even other products are commonly formed during the reaction [2]. Since the secondary amine and tertiary amine are employed only to limited extent in the preparation of cation-active tensides [3], most studies are focused on primary amines. Although the Ni- and Co-based catalysts are most frequently employed during the nitrile hydrogenation to primary amines [4–7], most of them are not suitable for the title reaction due to the low selectivity to $C_2H_5NH_2$. Up to now, a great number of attempts have been made to achieve an as high as possible selectivity to the desired $C_2H_5NH_2$ [8]. Obviously, the catalyst plays a decisive role in determining the

* Corresponding author. Tel.: +86-21-6432-2272; fax: +86-21-6432-2142.
E-mail address: hexing-li@shtu.edu.cn (H. Li).

0920-5861/$ – see front matter © 2004 Elsevier B.V. All rights reserved.
doi:10.1016/j.cattod.2004.06.128

selectivity. During the past decades, amorphous alloys have been widely used in the hydrogenation owing to their higher activity, better selectivity, and stronger poisoning resistance [9–12]. We report here the Co-B and Ni-B amorphous alloys with the attempts to design highly effective catalysts for the CH_3CN hydrogenation to $C_2H_5NH_2$. Their catalytic behaviors are investigated and compared with each other and also with those of the corresponding crystallized Ni-B and Co-B catalysts and even Raney Ni. Based on the characterizations, the relationship between the catalytic performance and the structural properties of the catalysts was discussed briefly.

2. Experimental

2.1. Catalyst preparation

The M-B samples (M = Ni or Co) in the form of ultrafine particles were prepared by chemical reduction according to the method described in our previous papers [13,14]. Briefly, 48 ml 2.0 M KBH_4 solution containing 0.20 M NaOH was added dropwise into 30 ml aqueous solution of MCl_2 containing 1.5 g M under vigorous stirring. As the reduction is strongly exothermic, the KBH_4 solution was added very slowly (1.5 ml/min) and the reaction was performed at 273 K in the ice-water bath to prevent the local overheat which may cause the gathering of the small particles and/or the crystallization of the M-B amorphous alloy. The KBH_4 was greatly excessive and the reaction mixture was stirred for enough time to ensure the complete reduction of M^{2+} in the solution. The resulting black solid was washed free from Cl^- and K^+ ions with distilled H_2O (until pH = 7 was obtained). Then, it was further washed with absolute alcohol (EtOH) and finally, stored in EtOH until the time of use. Heating pretreatment of the M-B samples was carried out in N_2 flow at elevated temperatures from 298 to 773 K, each for 2.0 h, respectively. For comparison, Raney Ni catalyst was also prepared by alkali leaching the commercially available Ni-Al alloy (50 wt.% Ni, 200 meshes), as described elsewhere [15].

2.2. Catalyst characterization

The amorphous structure of the as-prepared catalysts was determined by X-ray powder diffraction (XRD, Bruker AXS D8-Advance with Cu Kα radiation), selective area electronic diffraction (SAED, JEM-2010), and extended X-ray absorption fine structure (EXAFS, BL-10B) carried out in the National Laboratory of High Energy Physics (KEK, Tsukuba, Japan). The crystallization process was followed by differential scanning calorimeter (DSC, Perkin-Elmer) under N_2 atmosphere at the heating rate of 10 K/min. The surface morphology and particle sizes were observed by a scanning electron micrograph (SEM, XL 30 Philips) and a transmission electron micrograph (TEM, JEM-2010). The bulk composition was detected by means of inductively coupled plasma (ICP, Jarrell-As Scan 2000). The active surface area (S_{act}) was determined by H_2 chemisorption, as described previously [16]. X-ray photoelectron spectroscopy (XPS) was performed on a Perkin-Elmer PHI 5000C ESCA system using Al Kα radiation to determine the surface electronic states and surface compositions according to the peak area and the sensitivity factors to B_{1s}, $Co_{2p_{3/2}}$, and $Ni_{2p_{3/2}}$ offered by Perkin-Elmer Company [17]. The sample was dried in situ in pure Ar atmosphere to minimize the surface oxidation. All the binding energy values were calibrated by using C_{1S} equal to 284.6 eV as a reference.

2.3. Activity test

Liquid phase hydrogenation of CH_3CN was carried out at 383 K in a 200 ml stainless autoclave containing 0.5 g catalyst, 10 ml CH_3CN, 30 ml EtOH, and 3.0 MPa H_2. In order to ascertain the role of mass transfer, the catalyst amount was varied from 0.5 to 2.0 g and the speed of agitation was varied from 1000 to 1700 rpm. In view of the observation that the reaction rate was independent of the stirring rate and that it varied linearly with catalyst amount (Fig. 1), it could be concluded that the stirring rate of 1000 rpm was high enough so that the hydrogenation rates were independent of mass transfer. The initial rate of reaction was obtained by measuring the drop of PH_2 within the first 0.5 h, from which both the specific activity (the H_2 uptake rate per g of M, R_H^m (mol/h g), where M refers to Ni or Co, respectively) and the areal activity (the H_2 uptake rate per m^2 of the active surface area, R_H^S (mol/h m^2)) were calculated by using the ideal gas equation. R_H^S could be considered as the intrinsic activity since the effect of metal dispersion has been excluded. During the reaction, the H_2 pressure was kept nearly constant and the reaction mixture was sampled every 60 min. The contents of various components were determined by using a gas chromatograph (GC 102) equipped with a FID from which both the conversion of CH_3CN and the selectivities to different products could be calculated. The conditions for the GC analysis were 2 m column filled with GDX-102/407, injector temperature 373 K, oven temperature 418 K, detector temperature 473 K, and carrier gas N_2, 30 ml/min. The reproducibility of the results was checked by repeating the runs at least three times on the same batch of catalyst and for another three times for a different batches of catalyst and was found to be within acceptable limits (±5% for the same batch of the catalyst and ±10% for the different batches of the catalyst).

3. Results and discussion

3.1. Structural and electronic characteristics of the as-prepared catalysts

The TEM morphologies, as shown in Fig. 2, demonstrated that both the Ni-B and Co-B amorphous alloys were present

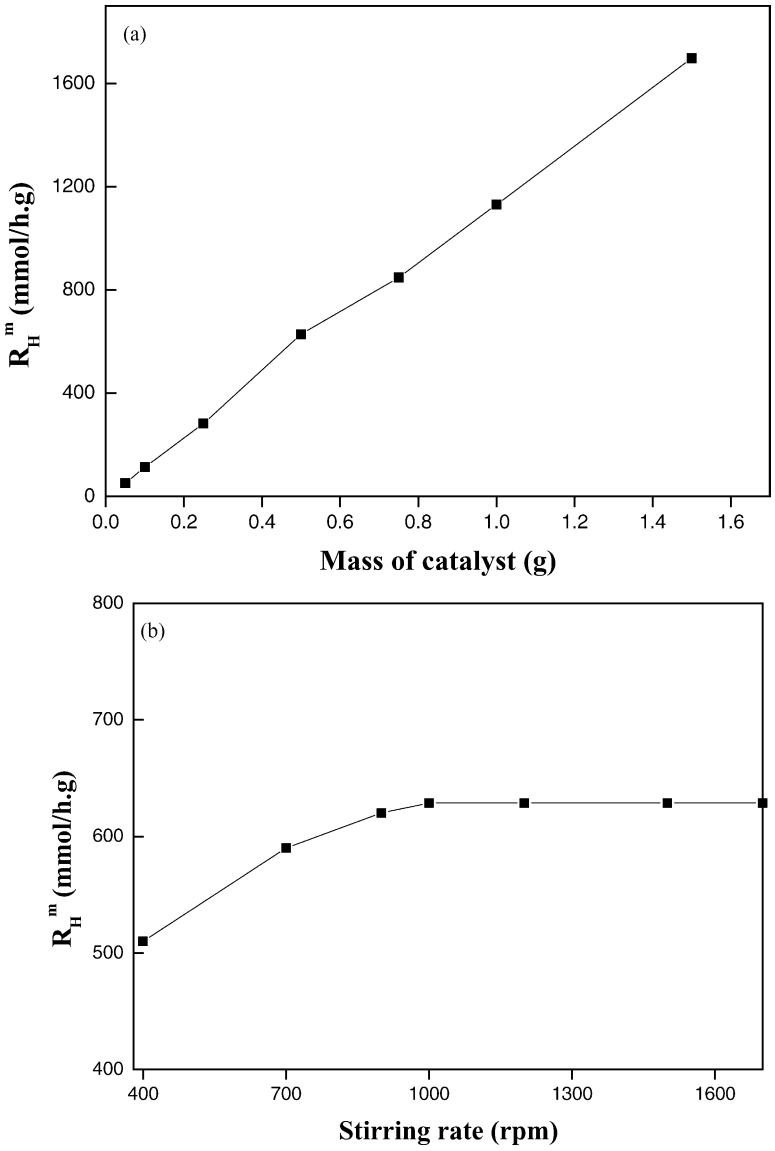

Fig. 1. Dependence of the initial hydrogenation rate (R^m) on: (a) the mass of the Co-B amorphous catalyst and (b) the stirring rate. Reaction conditions: 10 ml CH_3CN, 30 ml EtOH, $T = 383$ K, $P_{H_2} = 3.0$ MPa. (a) The stirring rate = 1000 rpm, (b) the mass of catalyst = 0.50 g.

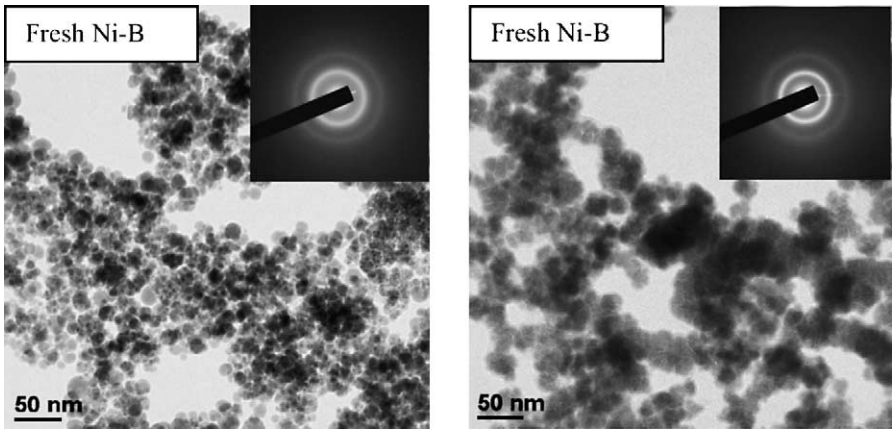

Fig. 2. TEM and SAED images of the fresh Co-B and Ni-B samples.

in the form of ultrafine spherical particles with the average diameters around 8.8 and 10.2 nm, respectively. The SAED pictures attached to Fig. 2 displayed a series of diffractional cycles indicative of typical amorphous structure [18] for both the fresh Ni-B and Co-B samples, from which these diffractional cycles may disappear and only separated bright dots could be observed after the samples being treated at 773 K for 2 h. The XRD patterns, as shown in Fig. 3, also demonstrated that both the fresh Co-B and Ni-B samples were present in amorphous structure since only one broad peak around $2\theta = 45^\circ$ was observed for each sample, respectively [19,20]. Concerning the Ni-B sample, one can see that no significant change in its XRD pattern occurred when the sample was treated at temperature below 573 K. However, heat treatment at temperature above 573 K resulted in various crystalline diffractional peaks corresponding to metallic Ni, Ni_2B and Ni_3B. The strength and the number of the diffractional peaks increased rapidly with the increase of the treating temperature up to 633 K. Then, the XRD pattern remained nearly unchanged even when the treating temperature was further enhanced. These results suggested that the Ni-B amorphous alloy started to be crystallized at 573 K and reached to completion at 633 K. Deep decomposition of the Ni-B alloy occurred during the crystallization process since only metallic Ni phases were observed after complete crystallization. Similar phenomena were also observed for the Co-B sample during the heating treatment. However, the Co-B amorphous alloy began to be crystallized at 623 K and reached to complete crystallization at 703 K, showing that the Co-B amorphous alloy had much better thermal stability. The DSC analysis, as shown in Fig. 4, further confirmed that the crystallization temperature of the Co-B amorphous alloy was nearly 150 K higher than that of the Ni-B amorphous alloy.

Fig. 5 shows the RDF curves of Co-B and Ni-B samples obtained by the fast Fourier transformation from the EXAFS data. The principal peaks could be attributed to the Ni–Ni or Co–Co interaction while the shoulder peak could be attributed to the Ni–B or Co–B interaction [21]. Obviously, both the fresh Ni-B and Co-B samples displayed typical amorphous structure, i.e. no long-range ordering but only

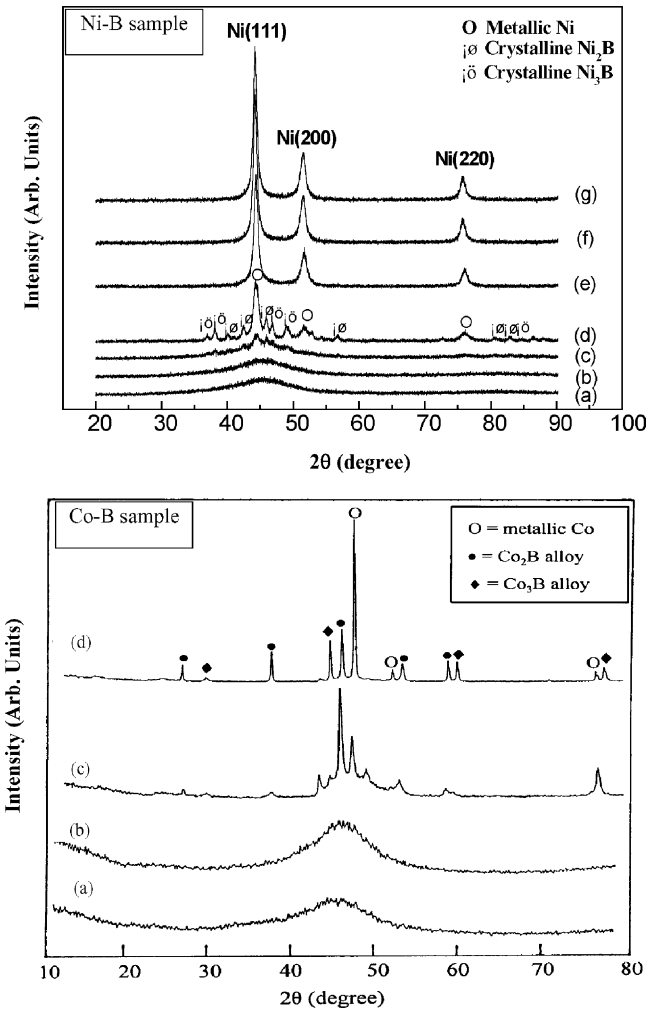

Fig. 3. XRD patterns of the Ni-B sample treated at (a) 298 K, (b) 533 K, (c) 553 K, (d) 573 K, (e) 593 K, (f) 613 K, (g) 633 K, each for 15 min, respectively, and the Co-B sample treated at (a) 298 K, (b) 473 K, (c) 673 K, (d) 773 K, each for 2 h, respectively.

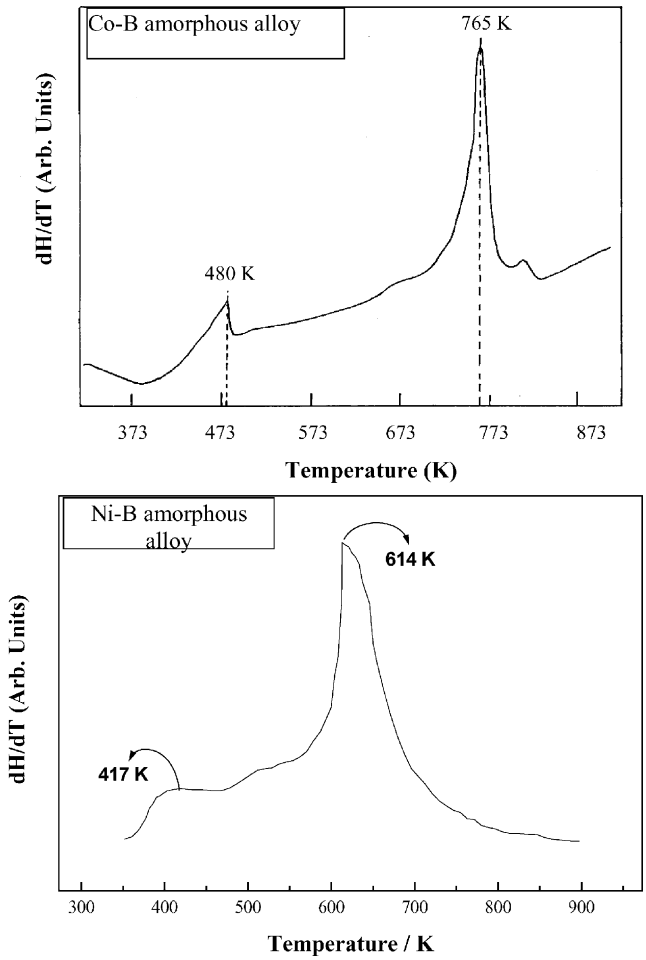

Fig. 4. DSC profiles of the Co-B and Ni-B amorphous alloy catalysts.

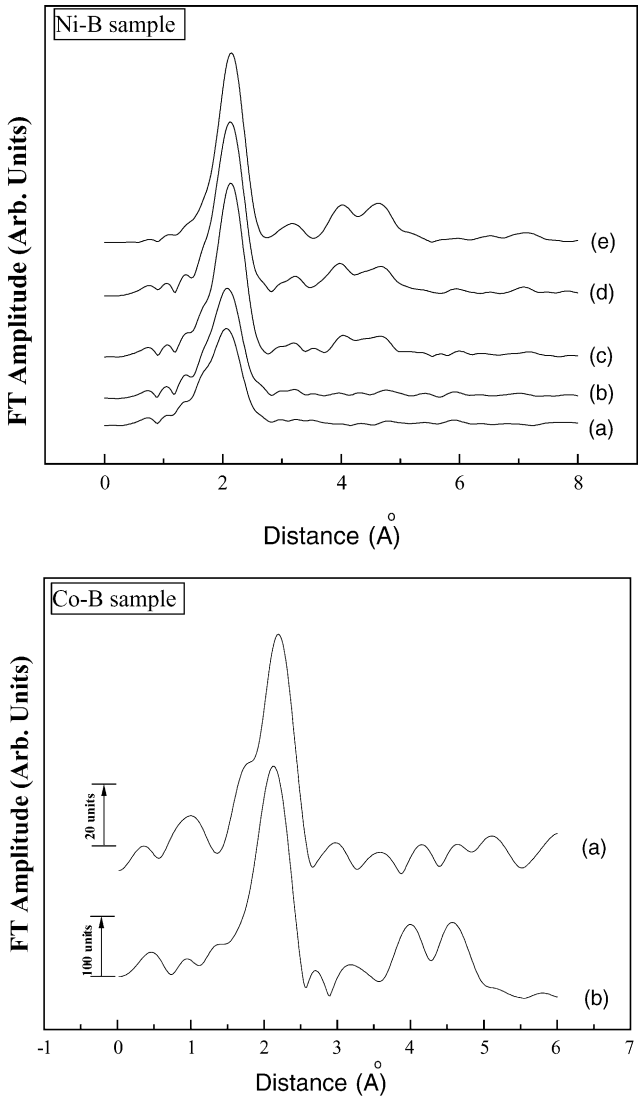

Fig. 5. RDF curves of the Ni-B sample treated at (a) 298 K, (b) 373 K, (c) 523 K, (d) 623 K, (e) 773 K, and the Co-B sample treated at (a) 298 K and (b) 773 K, each for 2 h, respectively.

short-range ordering structure, since only one weak FT peak around $R = 2$ Å was observed. After being treated at 773 K for 2 h, the intensity of the original peak increased profoundly and two small additional peaks appeared at longer distances, showing the transformation from an amorphous structure to a well-ordered crystalline structure.

From the XPS spectra (Fig. 6), one can see that, for both the fresh Ni-B and Co-B samples, nearly all the nickel and cobalt species were present in the metallic state corresponding to binding energy (BE) of 778.3 eV in $Co_{2p_{3/2}}$ level and 853.0 eV in $Ni_{2p_{3/2}}$ level, respectively. However, the boron species were present in two states, the elemental B alloying with metallic Ni or Co corresponding to BE of 188.2 eV and the oxidized B to BE of 192.5 or 192.1 eV. In comparison with the standard BE value of the pure B (187.2 eV) [17], one can see that the BE of the alloying B in either Ni-B or Co-B sample was positively shifted. Chen [9] also observed the positive BE shift of the alloying B in the Ni-B amorphous alloy. They believed that partial electrons transferred from the alloying B to oxygen in the neighboring B_2O_3 rather than to the metallic Ni since the electronegativity of B is much higher than Ni. On contrary, the alloying B accepted partial electrons from the metallic Ni. They supplied excellent experimental results to support their conclusion, which showed that the CO adsorption produced higher heat on K^+/Ni than on the Ni, while the CO adsorption on the Ni-B amorphous alloy produced lower heat than on the Ni. These results have been confirmed by our experiments. As the K^+ donates electrons to Ni, it seems quite natural to conclude that the alloying B might attract electrons from the Ni. However, we think that the above conclusion about the electronic interaction might not be exactly true due to the different roles of K^+ and B in the K^+/Ni and Ni-B, respectively. As well known, the K^+ donated electrons to the Ni in the K^+/Ni, but it did not change the structure of Ni active center. However, the role of alloying B in the Ni-B was much more complex. Besides the electron interaction, modification with alloying B may also change the structural characteristics of the Ni active sites. For example, the Ni-B alloy was present in amorphous structure while the K^+/Ni was still in the crystalline form. The alloying between B and Ni may also change some structural parameters, as well discussed below. The change of these structural properties might also change the CO adsorption heat on the Ni active center and even the adsorption model. Therefore, it might not be convincing to conclude the electron transfer between Ni and B in the Ni-B amorphous alloy by simply comparing the CO adsorption heat on the K^+/Ni and the Ni-B sample because the former might be attributed to merely the electronic interaction between K^+ and Ni while the latter might be attributed to both the electronic interaction between Ni and B and the structural modification of the Ni active center by the alloying B. Here, we suggested that the alloying B donated partial electrons to the metallic Ni or Co in the Ni-B or Co-B amorphous alloy based on the following evidences: (a) a mixture of elemental B and B oxide was prepared by decomposing the KBH_4 in acidic solution in the presence of Cu^{2+}. Unlike Ni-B amorphous alloy, the XRD patterns demonstrated that all the Cu species were present in pure metallic state (crystalline Cu) without forming Cu-B alloy. Under that case, no significant BE shift of the B was observed from the XPS spectra, implying that the positive BE shift of the elemental B was mainly electron-donation of B to the alloying metal, rather than to the neighboring B_2O_3. (b) The Ni-B amorphous alloy obtained by chemical reduction with KBH_4 always contains comparable oxidized B species due to the decomposition of KBH_4 in aqueous solution. To diminish their effect on the BE of alloying B, the Ni-B alloy prepared by the rapid quenching technique was employed. Such Ni-B alloy possessed the similar amorphous structure to the Ni-B amorphous alloy prepared by chemical reduction, but it contained very little or even no oxidized B species since the preparation was performed

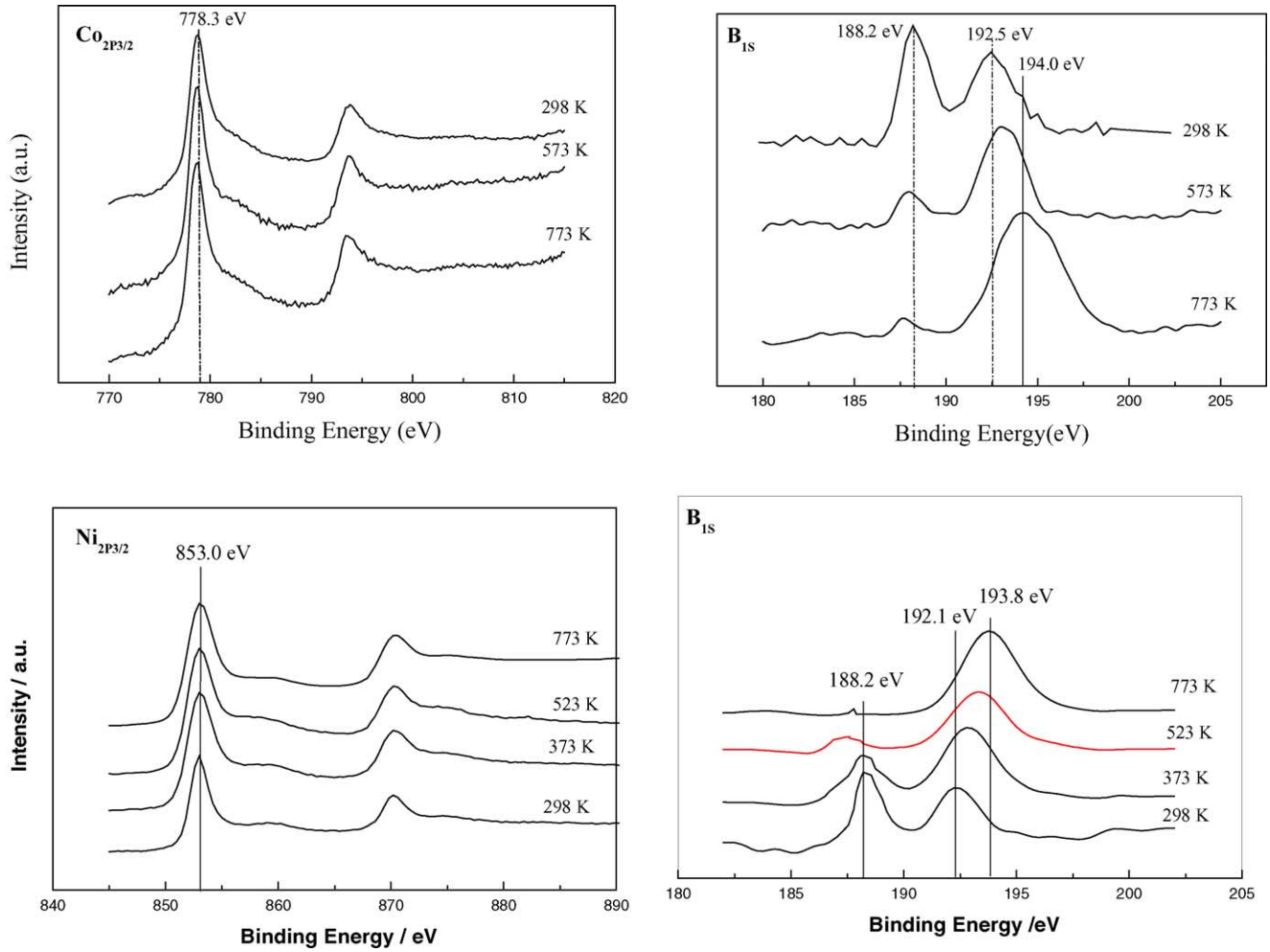

Fig. 6. XPS spectra of the Co-B and Ni-B samples treated at different temperatures.

exactly in the absence of O_2. Trace oxidized species on the surface were further removed by washing dilute HNO_3. However, as found by Yoshida et al. [22], the XPS spectra also revealed the positive BE shift of the alloying B, which was obviously due to its electron donation to the metallic Ni in the Ni-B alloy since no other species were present at all. (c) The theoretical calculations using ab initio DFT method also demonstrated that the alloying B donated partial electrons to Ni in the M-B amorphous alloy regardless the model of M-B clusters (M_xB_2, $x = 1$–4), as shown in Table 1. (d) As reported in our previous paper [23], the alloying B in the Ni-B amorphous alloy could effectively protect the metallic Ni from oxidation. A reasonable explanation might be the electron donation of the alloying B, making the metallic Ni electron-enriched which resisted the oxidation. Thus, as widely accepted [22,24,25], we suggested that partial electrons transferred from the alloying B to the metallic Ni or Co in their amorphous alloys, making these metals electron-enriched while the alloying B electron-deficient. Such electron transfer has been successfully explained by Imanaka et al. who suggested that the bonding electrons of the alloying B occupied the vacant d-orbitals of metallic Ni or Co [26]. The failure in observing the BE shift of the metallic Ni or Co could be understood by considering its relatively greater atomic weight comparing to that of the B atom [27].

Table 1
The electron populations of Ni and B atoms in M_xB_2 (M = Co or Ni) clusters[a]

M-B model	B [1]	B [2]	Ni [1]	Ni [2]	Ni [3]	Ni [4]
M_2B_2	+0.2812	+0.2812	−0.2812	−0.2812		
M_3B_2	+0.2301	+0.2301	−0.1652	−0.1475	−0.1475	
M_4B_2	+0.2962	+0.2962	−0.1481	−0.1481	−0.1481	−0.1481

[a] The symbols "+" and "−" represent electron-deficient and -enriched, respectively.

The XPS spectra in Fig. 6 also demonstrated that the content of alloying B decreased while the amount of the oxidizing B increased during the heating treatment, possibly due to the surface oxidation of the alloying B by trace oxygen in N_2 flow at high temperature. However, no significant oxidation of either metallic Ni or metallic Co was observed during the heating treatment, showing that the presence of the alloying B could effectively protect the surface Co or Ni from oxidation [23]. In addition, the BE of the alloying B gradually shifted down to 187.2 eV during the heating treatment due to the decomposition of the M-B alloys, as confirmed by the aforementioned XRD patterns. Besides the change of the BE value of alloying B, the positive BE shift of the oxidized B from 192.5 to 194.0 eV was also observed during the heating treatment. This could be interpreted in terms of the transformation from BO_2^- to B_2O_3. The standard BE values of these two species are 192.0 and 193.5 eV, respectively.

From the peak area in the XPS spectra and the corresponding sensitive factors, the surface B contents in the M-B amorphous alloys were calculated. As shown in Table 2, the surface B content was much higher than the bulk B content determined by the ICP analysis, showing that both Ni-B and Co-B amorphous alloys were surface-enriched with the boron species. Meanwhile, one can also see that the Co-B amorphous alloy was even more surface-enriched with the boron species.

Table 2 also revealed that the crystallization had no appreciable influence on the bulk composition of either the Ni-B or the Co-B sample. But great decrease in the surface B content was observed. In the crystallized Ni-B and Co-B samples, the surface B content was almost the same as the bulk B content. Meanwhile, the crystallization also caused an abrupt decrease in S_{act}, showing the agglomeration of the small Ni-B and Co-B alloy particles at high temperature, which could be confirmed by SEM morphologies. As shown in Fig. 7, the fresh Co-B and Ni-B samples were present in the form of ultrafine particles with homogeneous distribution. However, big lumps appeared and the particle size increased remarkably after crystallization. It seems that the Co-B amorphous alloy had much stronger resistance to sintering during the heating treatment since the average particle size of the crystallized Co-B was smaller than that of the crystallized Ni-B catalyst, which could also account for its higher S_{act} (see Table 2).

3.2. Hydrogenation activities

The hydrogenation activities of the as-prepared catalysts during the liquid phase hydrogenation are summarized in Table 2. Both the Co-B and Ni-B samples exhibited much higher activity than their corresponding crystallized counterparts obtained by treating the fresh Co-B and Ni-B samples at 773 K for 2 h in N_2 flow. Partially, it could be attributed to the abrupt decrease of the S_{act}. However, the more important reason might be the remarkable decrease in the intrinsic activity (R_H^S) which could be mainly attributed to the electronic effect. As mentioned above, the XPS spectra demonstrated that the metallic Co or Ni in the Co-B and Ni-B amorphous alloys was electron-enriched while the alloying B was electron-deficient. After crystallization, such electronic interaction decreased or even disappeared due to the decomposition of the amorphous alloy, as shown in the XRD patterns. The relative high density of electrons on the Ni or Co active sites may weaken their adsorption strength for CH_3CN molecules by repelling the lone electron pair on the nitrogen atom in the cyano (C≡N) group. This was favorable for the competitive adsorption for H_2 and more H_2 could be adsorbed. Kinetic studies revealed that the CH_3CN hydrogenation over either the Co-B and Ni-B amorphous catalyst was first-order with respect to hydrogen pressure while zero-order to CH_3CN concentration, as shown in Fig. 8. Thus, the increase of the adsorbed hydrogen could enhance the hydrogenation activity. In addition, according to the adsorption model of the nitrile [28], the electronic interaction between the C≡N group and the metallic Co or Ni active sites was the forward donation of the electrons from the highest occupied molecular orbital (HOMO) of the C≡N bonding, i.e., from the $\pi_{C\equiv N}$ to the d_{Z^2} and s orbitals of the metallic atom, and the back donation from the $d_{x^2-y^2}$ orbital of the metallic atom to the lowest unoccupied molecular orbital (LUMO), i.e. $\pi^*_{C\equiv N}$. Certainly, increasing the back donation might favor the C≡N bond dissociation since the $\pi^*_{C\equiv N}$ was an anti-bonding orbital, making the C≡N bond activated toward hydrogenation. Furthermore, the electron-enriched Co or Ni may also inhibit their adsorption for $C_2H_5NH_2$ and/or $(C_2H_5)_2NH$, retarding the poisoning of the catalysts by amines products [8].

Concerning the different Ni-based catalysts, one can see that, although Raney Ni exhibited very high R_H^m ow-

Table 2
Structural and catalytic properties of the as-prepared catalysts[a]

Catalyst	Bulk comp. (atom%)	Surf. comp. (atom%)	S_{act} (m^2/g)	$\bar{d}$ (nm)	R_H^m (mmol/h g)	R_H^S (mmol/h m^2)
Fresh Co-B	Co75.4B24.6	Co53.9B46.1	15.8	10.2	628.7	39.5
Fresh Ni-B	Ni75.0B25.0	Ni66.6B33.4	19.6	8.8	859.6	43.8
Cryst.[b] Co-B	Co75.4B24.6	Co74.0B26.0	2.8	376	42.6	15.2
Cryst.[b] Ni-B	Ni75.0B25.0	Ni74.2B25.8	0.43	566	9.0	20.9
Raney Ni	Ni	Ni	46.0	–	1322	28.7

[a] Reaction conditions: 0.5 g catalyst, 10 ml CH3CN, 30 ml EtOH, $T = 383$ K, $P_{H_2} = 3.0$ MPa, stirring rate = 1000 rpm.
[b] Crystallized Ni-B and Co-B samples obtained by treating the fresh samples at 773 K for 2 h.

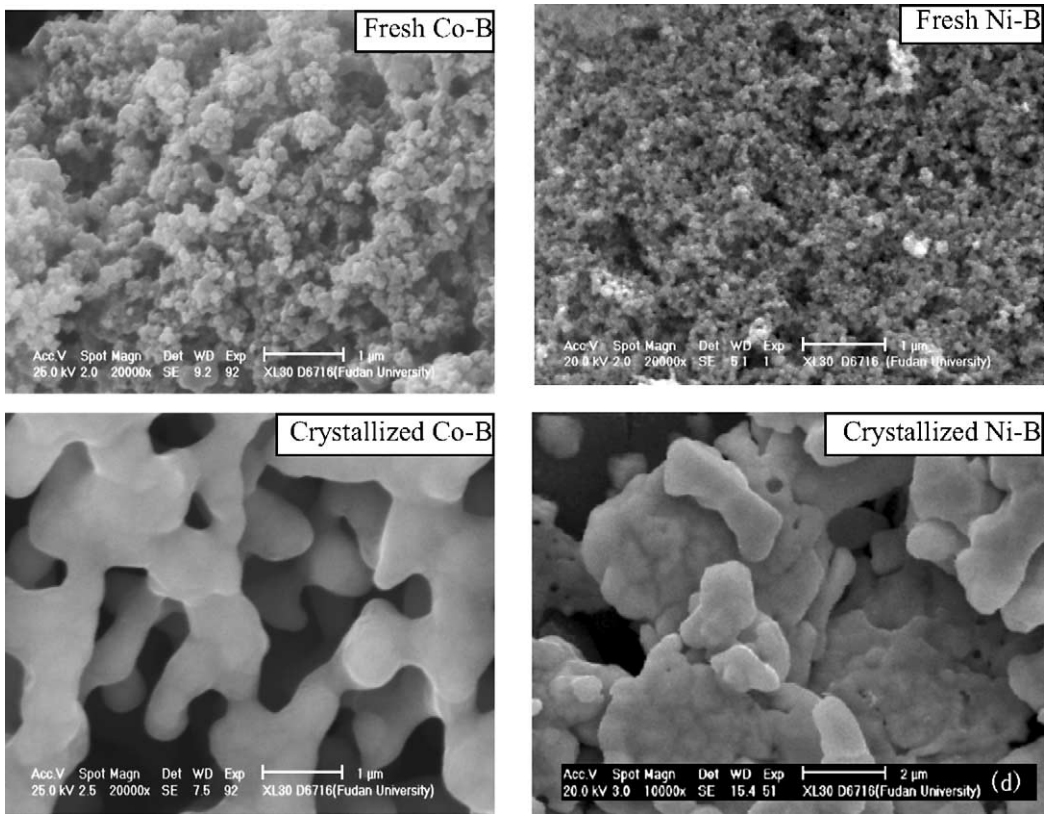

Fig. 7. SEM morphologies of the amorphous and crystallized Co-B or Ni-B catalysts.

ing to the larger S_{act}, its lower R_H^S demonstrated that the Ni active sites in Raney Ni were less active than those in the Ni-B amorphous alloy. Similar to that of the crystallized Ni-B catalyst, the lower R_H^S of Raney Ni could be attributed to the absence of either the amorphous structure or the electronic interaction between metallic Ni and the alloying B.

The Ni-B amorphous alloy exhibited higher activity (both R_H^m and R_H^S) than the Co-B amorphous alloy, showing the Ni was more active than the Co for the CH_3CN hydrogenation. As discussed above, both two catalysts were present in the amorphous structure with nearly the same structural parameters. Thus, the difference in their activities lied essentially in the properties of the metallic Ni and Co themselves. The lower activity of the Co catalysts was possibly due to its stronger adsorption for the CH_3CN [29] which may inhibit the competitive adsorption of hydrogen. As the CH_3CN hydrogenation was first-order with respect to hydrogen and zero-order to CH_3CN, the less adsorption of hydrogen on the Co actives sites could account for the lower activity of the Co-B amorphous alloy. Although the Co-B amorphous catalyst possessed lower activity, it exhibited much stronger durability during the CH_3CN hydrogenation since no significant decrease in activity was observed when it was used repetitively for 10 times. However, under the same conditions, the Ni-B amorphous alloy and Raney Ni catalysts could be used, repetitively, only for six and two times. Addition of little water could increase the lifetime of the catalysts. Taking into account that water could form hydrogen bonding with amine group and in turn may inhibit its adsorption on the active sites [30], it was reasonable to deduce that the deactivation of the catalysts was mainly due to the poisoning effect of the products including $C_2H_5NH_2$ and/or $(C_2H_5)_2NH$. The longer lifetime of the Co-B amorphous alloy may be attributed to the stronger adsorption for the reactant CH_3CN by Co active sites than that by Ni active sites. Such adsorption was so strong that no $C_2H_5NH_2$ could be adsorbed by Co active sites in the presence of CH_3CN [8]. Therefore, only $(C_2H_5)_2NH$ could act as a poison for the Co-based catalysts while both $C_2H_5NH_2$ and $(C_2H_5)_2NH$ may poison the Ni active sites.

3.3. Selectivities to ethylamine

Fig. 9 illustrated the change in the composition of the reaction mixture as a function of proceeding time during the liquid phase CH_3CN hydrogenation. Besides $C_2H_5NH_2$ (primary amine) as the main product, only $(C_2H_5)_2NH$ (secondary amine) was identified throughout the reaction process. Over the Co-B amorphous alloy, the content of $(C_2H_5)_2NH$ increased much more slowly than that over either the Ni-B amorphous alloy or Raney Ni catalyst. The maximum yields of $C_2H_5NH_2$ over Co-B, Ni-B and Raney were 93.5, 68.1 and 37.3%, respectively, and thus,

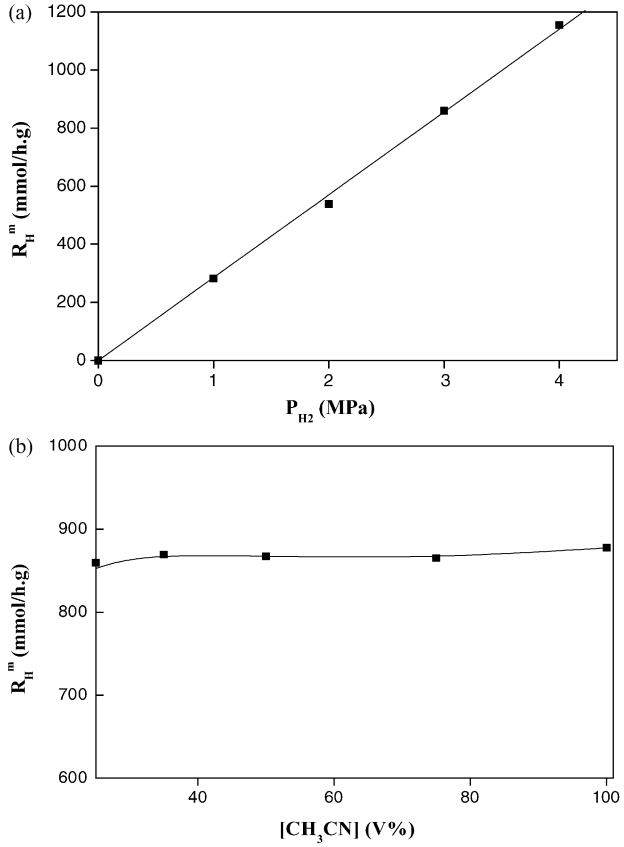

Fig. 8. Effects of: (a) the hydrogen pressure and (b) the acetonitrile concentration on the initial rate of acetonitrile hydrogenation per gram Ni (R_H^m) over the Ni-B amorphous catalyst. Reaction conditions: 0.50 g catalyst, 10 ml CH_3CN, 30 ml EtOH, $P_{H_2} = 3.0$ MPa, $T = 383$ K, stirring rate = 1000 rpm.

the selectivity to $C_2H_5NH_2$ changed in the order of Co-B amorphous alloy > Ni-B amorphous alloy > Raney Ni.

According to the above Braun's mechanism [8], as shown in the following scheme:

$$CH_3C{\equiv}6;{=}N \xrightarrow{+H_2} CH_3CH{=}CH \xrightarrow{+H_2} CH_3CH_2NH_2 \quad (R1)$$

$$CH_3CH{=}NH + CH_3CH_2NH_2 \xrightarrow{-NH_3} CH_3CH{=}NCH_2CH_3 \xrightarrow{+H_2} CH_3CH_2NHCH_2CH_3 \quad (R2)$$

the selectivities to $C_2H_5NH_2$ and $(C_2H_5)_2NH$ were mainly dependent on the competition between the hydrogenation of the $CH_3CH{=}NH$ leading to $C_2H_5NH_2$ and the condensation of $CH_3CH{=}NH$ with $C_2H_5NH_2$ leading to $(C_2H_5)_2NH$ [31]. The higher hydrogenation rate and the lower condensation rate lead to the better selectivity toward $C_2H_5NH_2$. Such assumption could account for the order of selectivity to $C_2H_5NH_2$ over different catalysts. On one hand, the better selectivity of the Ni-B amorphous alloy than that of Raney Ni was mainly attributed to the electronic interaction

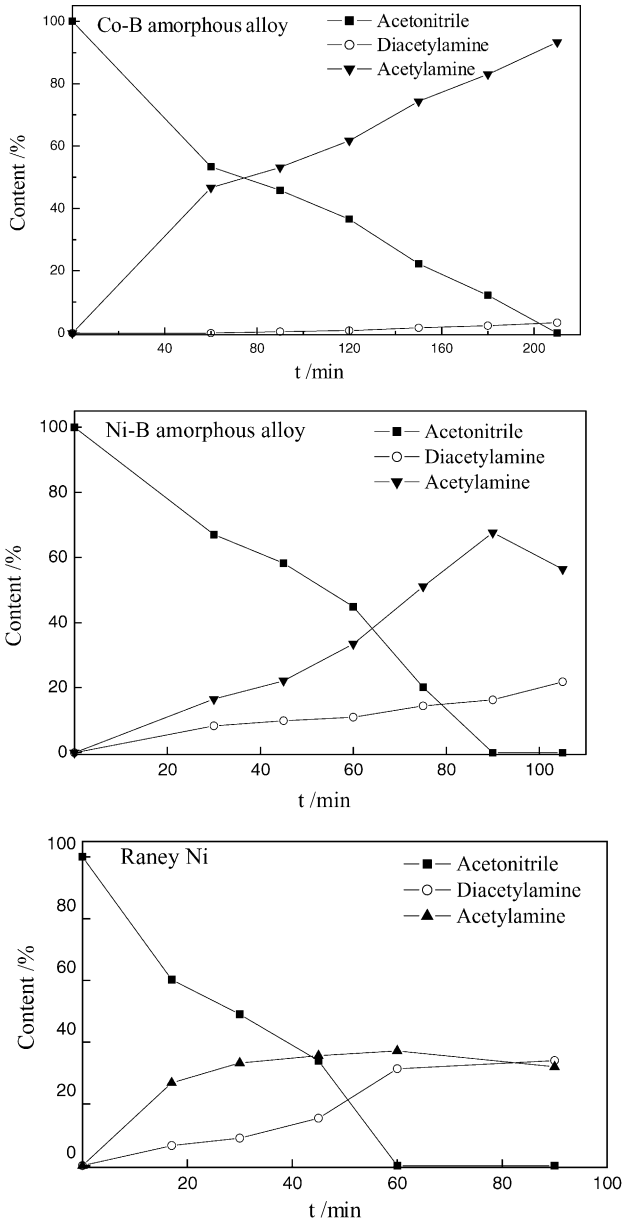

Fig. 9. Dependence of the composition of the reaction mixture on the reaction time during the liquid phase acetonitrile hydrogenation over different catalysts. Reaction conditions are given in Fig. 8.

between metallic Ni and alloying B. As the condensation between $CH_3CH{=}NH$ and $C_2H_5NH_2$ should occur on the catalyst surface [8], the adsorption for both $CH_3CH{=}NH$ and $C_2H_5NH_2$ was essential. Owing to the electron-donation by the alloying B, the Ni active sites in the Ni-B amorphous alloy possessed higher electron density which could effective repel the lone pair electrons on the N atom in the $C_2H_5NH_2$ molecule and in turn, weaken the $C_2H_5NH_2$ adsorption. Thus, the condensation between the $C_2H_5NH_2$ and the $CH_3CH{=}NH$ could be inhibited since less $C_2H_5NH_2$ was adsorbed by Ni active sites. Meanwhile, as the condensation proceeded through a nucleophilic attack of the N atom in

the $C_2H_5NH_2$ molecule on the C atom connecting with the N atom in the $CH_3CH{=}NH$ molecule [32]:

the more positive charges on the C atom and the more negative charges on the N atom may facilitate the condensation reaction. The high electron density on the Ni active sites could increase the back donation of electrons from Ni to the $\pi^*_{C=N}$, making the C atom less positive and in turn, retarding the condensation reaction. Furthermore, the increase in the electrons back donation to the anti-bonding orbital ($\pi^*_{C=N}$) could also weaken the C=N bond, making the C=N bond activated toward hydrogenation and thus, also increased the selectivity to $C_2H_5NH_2$.

On the other hand, the superior selectivity of the Co-B amorphous alloy over that of the Ni-B amorphous alloy was mainly attributed its stronger adsorption for CH_3CN. As mentioned above, the adsorption for CH_3CN on the Co active sites was so strong that $C_2H_5NH_2$ could not be adsorbed in the presence of acetonitrile, i.e. before the total conversion of acetonitrile. Under that case, the condensation between $CH_3CH{=}NH$ and $C_2H_5NH_2$ was nearly completely inhibited since almost no $C_2H_5NH_2$ was present on the catalyst surface. In addition, although no BE shift of either Ni or Co in the Ni-B or Co-B amorphous alloy was observed from XPS spectra, the theoretical calculations using ab initio DFT method revealed that the Co and Ni may have different electron densities due to the different contents of alloying B. From Table 2, one can conclude that the surface composition of the Co-B amorphous alloy was similar to the model of Co_3B_2, while the Ni-B sample was similar to the model of Ni_4B_2. Thus, as shown in Table 1, the metallic Co in the Co-B alloy accepted more electrons from the alloying B than the metallic Ni in the Ni-B amorphous alloy. As discussed above, the more electron-enriched Co active sites were favorable for the hydrogenation of $CH_3CH{=}NH$ and unfavorable for the condensation between $CH_3CH{=}NH$ and $C_2H_5NH_2$, resulting in the high selectivity to $C_2H_5NH_2$.

4. Conclusion

This study reported five Ni- and Co-based catalysts used for the selective hydrogenation of CH_3CN to $C_2H_5NH_2$ in liquid phase, which seems helpful to design new powerful catalysts for the title reaction. More specially, the following points are highlighted:

(1) The amorphous alloys exhibited much higher activity and selectivity to $C_2H_5NH_2$, showing the promoting effects of both the amorphous structure and the alloying B. The higher activity of the amorphous alloys was interpreted in terms of both the structural effect and the electronic effect. However, the better selectivity to $C_2H_5NH_2$ was mainly attributed to the electronic effect.

(2) Although the Co-B amorphous alloy showed slightly lower activity in comparison with that of the Ni-B amorphous alloy, its excellent lifetime and selectivity to $C_2H_5NH_2$ as well as very high yield of $C_2H_5NH_2$ (93.5%) showed a good potential in industrial application. It could be predicted that the combination of Co-B and Ni-B amorphous alloys might result more powerful catalysts for the CH_3CN hydrogenation to $C_2H_5NH_2$. These works are being underway.

Acknowledgements

This work was supported by the National Natural Science Foundation of China (29973025), the Natural Science Foundation of Shanghai Science and Technology Committee and the Shanghai Education Committee (01DZ01).

References

[1] G.B. Kauffman, J. Chem. Educ. 65 (1988) 803.
[2] C.D. Bellefon, P. Fouilloux, Catal. Rev. -Sci. Eng. 36 (1994) 459.
[3] V.M. Lenfield, Cationic Surfactants, E. Jungermann (Ed.), New York, 1970.
[4] H. Greenfield, Ind. Eng. Chem. Prod. Res. Dev. 6 (1967) 142.
[5] J. Pasek, N. Kostova, B. Dvorak, Collect. Czech. Chem. Commun. 46 (1981) 1011.
[6] K. Weissermel, H.-J., Industrial Organic Chemistry, 2nd ed., VCH, Weinheim, 1993.
[7] D. Gavroy, C. Joly-Vuillemin, G. Cordier, P. Fouilloux, H. Delmas, Catal. Today 24 (1995) 103.
[8] J. Volf, P. Josef, Stud. Surf. Sci. Catal. 27 (1986) 105.
[9] Y. Chen, Catal. Today 44 (1998) 3.
[10] J.F. Deng, H.X. Li, W.J. Wang, Catal. Today 51 (1999) 113.
[11] A. Molnar, G.V. Smith, M. Bartok, Adv. Catal. 36 (1989) 329.
[12] A. Baiker, Faraday Discuss. Chem. Soc. 87 (1989) 239.
[13] H.X. Li, X.F. Chen, M.H. Wang, Y.P. Xu, Appl. Catal. A: Gen. 225 (2002) 117.
[14] H.X. Li, H. Li, W.L. Dai, M.H. Qiao, Appl. Catal. A: Gen. 238 (2003) 119.
[15] H.X. Li, W. Wang, H. Li, J.F. Deng, J. Catal. 191 (2000) 257.
[16] H.X. Li, W. Wang, H. Li, J.F. Deng, J. Catal. 194 (2000) 211.
[17] Operator's Reference Manual for PHI PC Windows Software Version 1.2b, Physical Electronic Division, Perkin-Elmer, pp. 274–285.
[18] S. Klein, J.A. Martens, R. Parton, K. Vercruysse, P.A. Jacobs, W.F. Maier, Catal. Lett. 38 (1996) 209.
[19] A. Yokoyama, H. Komiyama, H. Inoue, T. Masumoto, H.M. Kimura, J. Catal. 68 (1981) 355.
[20] H. Yamashita, M. Yoshikawa, T. Funabiki, S. Yoshida, J. Chem. Soc., Faraday Trans. I 82 (1986) 1771.
[21] B. Shen, S. Wei, K.N. Fan, J.F. Deng, Appl. Phys. A 65 (1997) 295.
[22] S. Yoshida, H. Yamashita, T. Funabiki, T. Yonezawa, J. Chem. Soc., Faraday Trans. 80 (1) (1984) 1435.
[23] W.L. Dai, H.X. Li, Y. Cao, M.H. Qiao, K.N. Fan, J.F. Deng, Langmuir 18 (2002) 9605.
[24] S.P. Lee, Y.W. Chen, J. Mol. Catal. A: Chem. 152 (2000) 213.

[25] Y. Okamoto, Y. Nitta, T. Imanaka, S. Teranishi, J. Catal. 64 (1980) 397.
[26] T. Imanaka, Y. Nitta, S. Teranishi, Bull. Chem. Soc. Jpn. 46 (1973) 1134.
[27] H. Li, H.X. Li, W. Dai, Z. Fang, J.F. Deng, Appl. Surf. Sci. 152 (1999) 25.
[28] G.D. Yadav, M.R. Kharkara, Appl. Catal. A: Gen. 126 (1995) 115.
[29] M. Kalina, J. Pasek, Kinet. Catal. 10 (1969) 574.
[30] H. Greenfield, Ind. Eng. Chem. Prod. Res. Dev. 15 (1976) 156.
[31] M. Morak, F. Frsnak, Czech. Pat. 3 (1974) 152102.
[32] P.N. Rylander, L. Hasbrouck, Eng. Ind. Tech. Bull. 11 (1979) 19.